2017 NDIA GROUND VEHICLE SYSTEMS ENGINEERING AND TECHNOLOGY SYMPOSIUM
MODELING & SIMULATION, TESTING AND VALIDATION (MSTV) TECHNICAL SESSION
AUGUST 8-10, 2017 - NOVI, MICHIGAN

DIGITAL TWIN FOR TANK TRACK ELASTOMERS: PREDICTING SELF-HEATING AND DURABILITY

William V. Mars, PhD
Endurica LLC
Findlay, OH

Matthew Castanier, PhD
TARDEC
Warren, MI

David Ostberg
William Bradford
TARDEC
Warren, MI

ABSTRACT

In this work, Abrams tank track system T-158LL backer pad elastomer self-heating and fatigue behavior was characterized experimentally, and the backer pad design was digitally twinned to show how complex in-service conditions can be evaluated virtually.

The material characterization included measurement of the thermal properties and dissipative characteristics of the rubber compound, as well as its fatigue crack growth rate curve and crack precursor size. The analysis included 1) a structural finite element analysis of the backer pad in operation to obtain the load history, 2) a thermal finite element analysis to obtain steady-state operating temperature distribution within the backer pad, and 3) a thermo-mechanical fatigue analysis using the Endurica CL fatigue solver to estimate the expected service life and failure mode of the backer pad.

As validation, experiments were conducted on the backer pad to measure operating temperature, fatigue life, and failure mode over a matrix of loads and frequencies typical of service. Operating temperatures in a range from 125 °F to 350 °F were observed. Several failure modes occurred in backer pad tests, depending on the load and frequency. In cases where thermal runaway occurred, a thermal degradation mechanism was observed internally in the pad. Under less severe conditions, fatigue crack growth initiating near the "binocular" tubes was observed. Fatigue life was found in almost all cases to fall between 10^3 and 10^7 cycles. Thermal runaway predictions for the T-158LL backer pad were also validated against tests in cases where debonding of the rubber from the metal core occurred.

The digital twin of the backer pad yielded failure modes quite similar to those observed in experiments, and gave realistic estimates of operating temperature and fatigue life. The fatigue analysis methods developed under this project have since been applied commercially, and have proven effective in a wide range of elastomer applications. Future applications of the tools will include durability improvement initiatives, light-weighting efforts, and remaining life tracking for reliability programs.

INTRODUCTION

With qualification testing costs in the range 0.75 to 1.5 million dollars per iteration for the M1 Abrams Tank Track system (Figure 1), track system elastomers require vetting prior to qualification tests. Self-heating and durability of track system elastomers (Figure 2) must therefore be ensured prior to prototype production [1-3]. In this work, track system T-158LL backer pad elastomer self-heating and fatigue behavior was characterized experimentally, and the backer pad design was digitally twinned. A digital twin is a complete virtual representation of the backer pad, matching not only the pad's geometry, but also its mechanical, thermal and damage behavior. In this case, the digital twin is aimed at enabling vetting prospective pad designs with respect to complex in-service conditions to enable better design down-select decision making.

Figure 1. Abrams Tank with Elastomeric Track.

MATERIAL CHARACTERIZATION

Digital Twin implementation requires knowledge of the elastic, fatigue, and thermal behaviors of subject materials. These behaviors were measured via experiments on supplier-provided samples of the subject material. The characterization experiments were conducted at Axel Products, Inc.

Elastic Properties

Steady-state nonlinear elastic properties under finite strain cyclic loading were determined via experiments in 4 modes of deformation: simple, planar, and biaxial tension, and volumetric compression. A 2nd order Ogden [4-6] hyperelastic

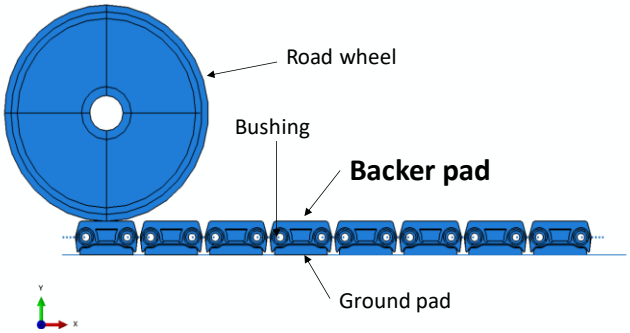

Figure 2. Track system elastomer components.

energy function has been used in this work to specify stress-strain behavior, with parameters as given in Table 1. The Ogden strain energy potential W is defined in equation (1) in terms of principal stretches $\bar{\lambda}_i$ and material parameters μ_i and α_i by

$$W = \sum_{i=1}^{N} \frac{2\mu_i}{\alpha_i^2}\left(\bar{\lambda}_1^{\alpha_i} + \bar{\lambda}_2^{\alpha_i} + \bar{\lambda}_3^{\alpha_i} - 3\right) \qquad (1)$$

Parameters describing the Mullins effect [7-8] (i.e. initial cyclic stress-softening) were also determined as shown in Table 1. The Mullins softening function η is defined for the strain energy function $\tilde{W}$ as given in equation (2)

$$\eta = 1 - \frac{1}{r}\,\mathrm{erf}\left[\frac{\tilde{W}(I_{1,\max}) - \tilde{W}(I_1)}{m + \beta\tilde{W}(I_{1,\max})}\right] \qquad (2)$$

r, m, β are material constants. $I_{1,\max}$ is the prior all-time maximum value of the first invariant of the Cauchy-Green Deformation tensor. I_1 is the current value of the first invariant.

Table 1. Stress-Strain Modeling Parameters

ELASTICITY_TYPE=O+MULLINS
MU1=2.275319e6 ! Pa
MU2=0.054452e6 ! Pa
ALPHA1=-1.00837
ALPHA2=7.863497
MULLINSR=6.641545796
MULLINSM=0.558478587e6 ! Pa
MULLINSBETA=0.029639767
BULK_MODULUS=140.7e6 ! Pa

Fatigue Properties

Fatigue performance of the subject material was determined via fatigue crack growth rate experiments on edge-cracked planar tension specimens [9-16]. The results of the experiments are shown in Figure 3. The Lake-Lindley crack growth rate law in equation (3) expresses the rate of crack growth r as a function of the energy release rate T of the crack. The Lake-Lindley law was calibrated based on these measurements, giving the parameters shown in Table 2.

$$r = r_c \left(\frac{T}{T_c} \right)^F \qquad (3)$$

The Lake-Lindley law is written in terms of 3 material parameters: the fracture mechanical strength T_c, the powerlaw slope F, and the value of the crack growth rate r_c, at which the powerlaw intersects a vertical asymptote located at T_c.

Table 2. Fatigue Modeling Parameters.

FATIGUE_TYPE=LAKELINDLEY
FLAWSIZE=15.7e-6 ! m
FLAWCRIT=1e-3 ! m
TCRITICAL=8342 ! J/m^2
THRESHOLD=117 ! J/m^2
TRANSITION=167 ! J/m^2
RC=0.5778e-3 ! m/cyc
F0=3.3486 !
TEMPCOEF=0.0506 ! 1/degC
TEMPREF=82.0 ! 1/ degC

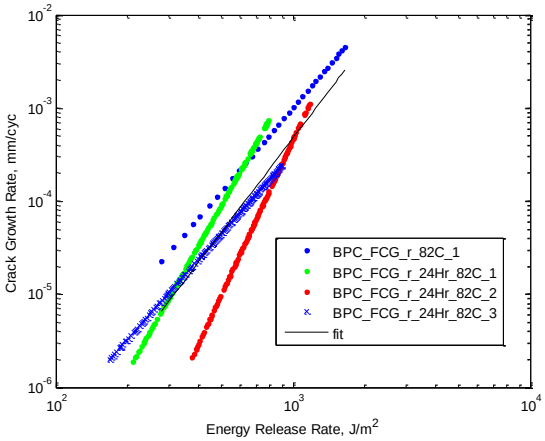

Figure 3. Fatigue crack growth rate measurements of the backer pad compound.

Thermal and Dissipation Properties

The thermal conductivity was determined experimentally as k = 3.34E-6 BTU / (s in °F). The density was ρ = 8.88E-5 lbm / in^3. The specific heat was C = 0.717 BTU / lbm °F.

Dissipative behavior of the elastomer was measured via dynamic experiments in which the energy loss per cycle (ie hysteresis) was observed for as many as 6 strain levels at 3 different temperatures (see Figure 4). The Endurica powerlaw dissipation model [17-20] was then fit to these results, giving the parameters in Table 3. The model involves the material parameters h_{ref}, ε_{ref}, γ, and θ_{ref}, and relates the strain ε to the hysteresis h.

$$h = h_{ref} \left(\frac{\varepsilon}{\varepsilon_{ref}} \right)^{\gamma} e^{r(\theta - \theta_{ref})} \qquad (4)$$

Table 3. Self-heating simulation parameters.

HYSTERESIS_TYPE=POWERLAW
TEMPCOEF=-0.0074 ! 1/degC
TEMPREF=82 ! degC
EREF=0.10
HYSREF=0.0095 ! mJ/mm^3/cyc
GAMMA=1.94
FSCALE=2.66
CHI=1.0

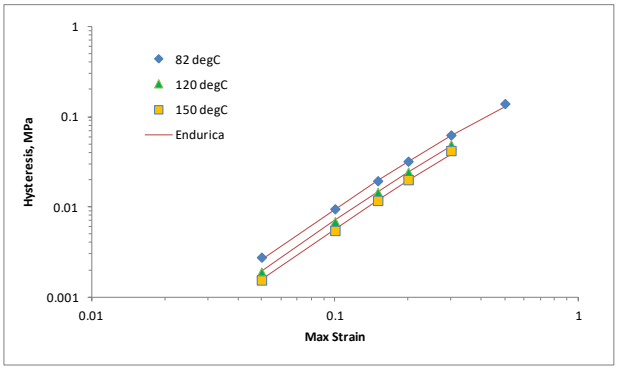

Figure 4. Self-heating law – model vs. experiment.

DIGITAL TWIN IMPLEMENTATION

The backer pad digital twin was implemented via the Abaqus solver for structural and thermal calculations, and the Endurica CL solver for dissipation and fatigue calculations. The digital twin was set to reflect the backer pad as it operates in a component durability test. The component test uses a single backer pad that is repeatedly brought into rolling contact with a rigid road wheel until the pad looses integrity. Note that in the component test, the bushings and ground pad, normally present when installed on the M1, are not included. The bushings and ground pad were also excluded from the digital twin.

As validation, fatigue experiments were conducted on the backer pad to measure operating temperature, fatigue life, and failure mode over a matrix of loads and frequencies typical of service. Two load levels were executed: 5400 lbf and 6700 lbf. These loads correspond approximately to upper and lower bounds of the range of loads that a ground pad sees under each of the M1 track system 7 road wheel stations as the vehicle is operated on pavement at high speeds [3], under the assumption that the load inboard and outboard are carried equally. Three frequency levels were executed: 6, 7, and 8 Hz. These frequencies correspond to vehicle operation at 30, 35, and 40 mph, where the loading caused by each of the 7 wheel stations is considered a single loading event. The matrix of operating conditions shown in Table 4 was executed via experiments and via simulation.

Table 4. Operating conditions for analysis and testing.

C1 5400 lbf, 6 Hz	B2 6700 lbf, 6 Hz
B3 5400 lbf, 7 Hz	B4 6700 lbf, 7 Hz
C5 5400 lbf, 8 Hz	B6 6700 lbf, 8 Hz

The analysis included 1) a structural finite element analysis of the pad in operation through one wheel traversal to obtain the load history, 2) a thermal analysis to obtain steady-state operating temperatures within the pad, and 3) a thermo-mechanical fatigue analysis using the Endurica CL fatigue solver to estimate the expected service life and failure model of the backer pad. The Endurica CL fatigue solver uses a microkinematic self-heating law [21] for estimating heat dissipation rates in the finite element model, and critical plane analysis for computing the fatigue life.

Structural Analysis

The finite element model of the track shoe consisted of 8454 nodes and 8099 reduced-integration, 2D plane strain elements. The model was supported at the center of each 'binocular tube' via an attachment to a rigid body, which was itself supported via a 1D spring and dashpot element attached to ground as shown in Figure 5. The mass of the rigid body, and the spring and dashpot rates were calibrated to produce a natural frequency matching the roughly 50 Hz 'ringing' signal observed in experiments due to the compliance of the testing frame on which fatigue experiments were conducted.

Loads on the elastomer backer pad were applied via a driven wheel as shown in the time series of Figure 6, with load and frequency specified in Table 4. Applied loads were reacted through a rigid connection between the test machine frame and the steel shoe 'binocular tubes'.

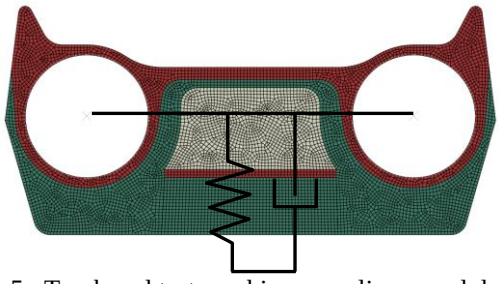

Figure 5. Track pad test machine compliance and damping were represented via a spring and dashpot. Red = Steel, White = Aluminum, Green = Rubber. Note that, as installed on the testing machine, the backer pad faces downward.

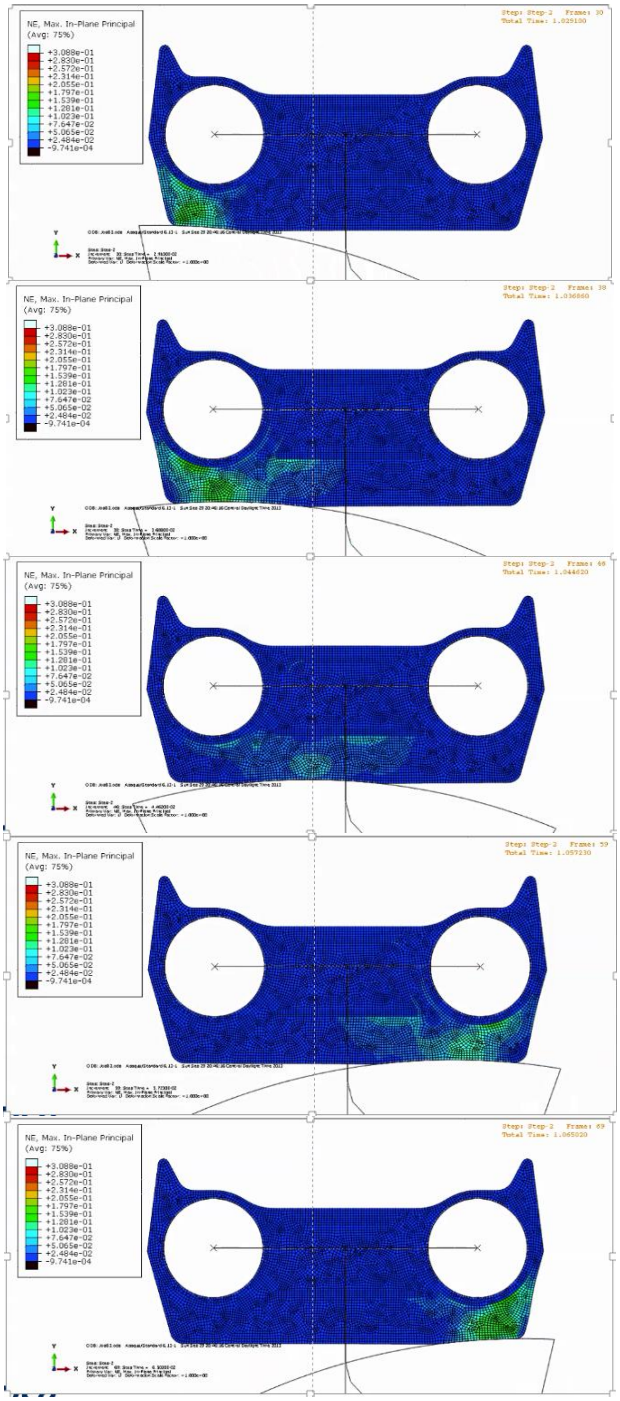

Figure 6. Time series showing rolling motion of road wheel in contact with track pad elastomer during component testing. Color contours show maximum principal nominal strain.

Self-Heating Analysis

Steady state operating temperatures were simulated in Abaqus, using heat dissipation rates computed with Endurica CL as part of the fatigue simulation.

The boundary conditions for the thermal FEA are shown in Figure 7. The heat transfer coefficient for the inner boundary was set by trial and error to represent the thermal resistance between the inner binocular tube and the ambient sink temperature of 72.5 °F. It was assumed constant in all cases, with a value of 3.4E-7 BTU/(in^2 s °F), since the thermal conductance path through the test machine frame does not change during testing. The heat transfer coefficient for the outer boundary was assumed to depend on test frequency (since the airspeed relative to the track pad depends on test frequency).

The following relationship was used to compute the outer boundary heat transfer coefficients given in Table 5.

$$h = h_0 \left| \frac{v}{v_0} \right|^{1/2}$$

$$h_0 = 35 \frac{\mathrm{W}}{\mathrm{m}^2\mathrm{K}} \qquad (5)$$

$$v_0 = 20 \frac{\mathrm{m}}{\mathrm{s}}$$

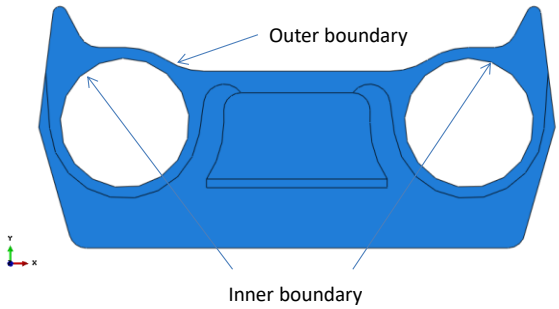

Figure 7. Thermal model boundary conditions.

Table 5. Outer boundary film coefficients.

Case	Freq (Hz)	Outer Boundary Film Coeff (Btu/in^2-s-F)
C1	6	3.1478e-6
B2	6	3.1478e-6
B3	7	3.4e-06
B4	7	3.4e-06
C5	8	3.6348e-6
B6	8	3.6348e-6

Dissipation rates for each finite element in the track pad were computed in Endurica CL, as part of the fatigue analysis, based on the powerlaw model shown in equation (4). Typical results are shown in Figure 8. The dissipation rates were computed via a directional model that considers the deformation history and energy losses produced by individual material lines and material slip planes of all possible orientations [22].

Given the boundary conditions, and Endurica-computed dissipations, the temperature distribution for each load case was computed. Since dissipation depends on temperature, an iterative calculation procedure was required. In general, convergence of the temperature field was obtained within 5 or 6 iterations.

Steady state thermal solutions for each operating case are shown in Figure 9. Higher loads and frequencies produce higher temperatures. The hottest internal location occurs where the road wheel first contacts the pad.

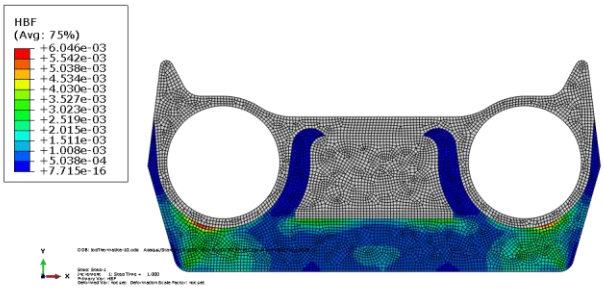

Figure 8. Typical computed distribution of volumetric dissipation rate.

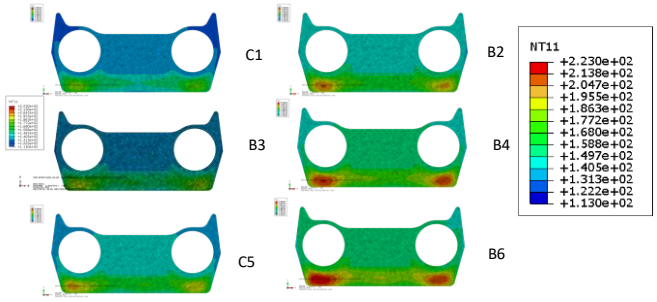

Figure 9. Computed steady-state temperature distribution for each operating case, degrees Fahrenheit.

Durability Analysis

Critical Plane Analysis [23-25] was used to compute the fatigue life, using the strain history and steady state temperature obtained from prior analysis steps. Critical Plane Analysis considers that crack development may occur in any orientation, and it identifies the particular plane on which the fatigue life (ie number of duty cycle repeats) is minimized. All fatigue calculations were made with the Endurica CL fatigue solver. Figure 10 shows the fatigue life distributions for each of the 6 operating scenarios, along with the average experimentally observed fatigue life. Cracking is predicted on the "binocular" tube / rubber interface, and in the "shoulders" of the pad.

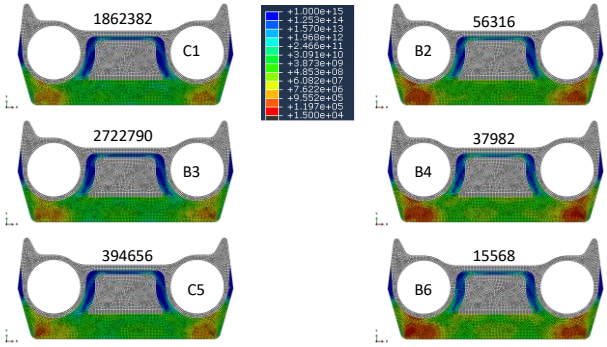

Figure 10. Computed fatigue life (red = short life, blue=long life). Experimental life is also noted for each case.

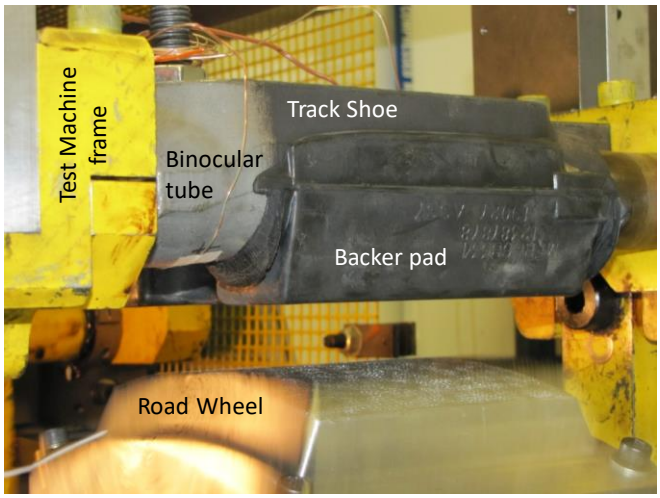

Figure 11. Track pad fatigue test machine.

COMPONENT TESTING

Track pad fatigue life and operating temperatures were evaluated experimentally on the testing machine shown in Figure 11. The track pad is mounted through the binocular tubes, and supported by the machine frame. The road wheel mechanism contacts and loads the track pad from below via a rolling motion that is driven at the frequencies specified in Table 4. Temperature measurements during the fatigue test were recorded via a thermocouple embedded in the aluminum core of the track pad (Core), and another on the steel binocular tube (Boundary).

The load history on the machine frame was recorded during test operation, and is shown for a typical case in Figure 12, which also overlays the load history computed in the finite element simulation. In addition to the main impact load which is driven at the primary frequency (in this case 7 Hz), the dynamics of the machine frame are seen to cause a 50 Hz 'ringing' signal. Both features of the loading signal were successfully captured in the finite element simulation.

In Figure 13, steady state operating temperatures for the Core and Boundary thermocouple positions are compared. Quite accurate predictions of the core temperature were obtained, with temperatures reaching as high as 160 °F for cases exhibiting a steady state solution. Accuracy for boundary temperatures was not as good, probably reflecting the limits of using a 2D finite element model to represent the 3D backer pad. The inaccuracy in the boundary temperature was tolerated in the digital twin because these temperatures occur on the outside of the steel shoe body, and they are irrelevant to durability of the backer pad.

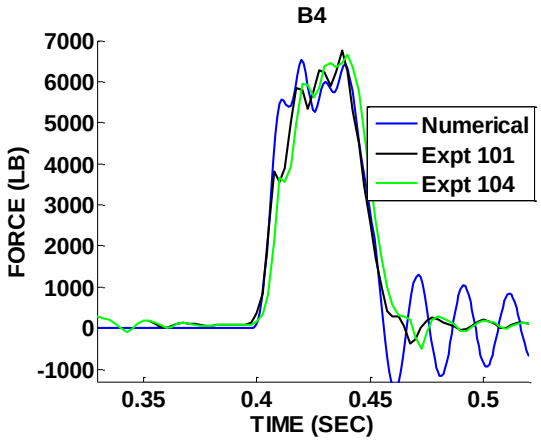

Figure 12. Typical comparison of observed vs modeled loads during track pad fatigue testing.

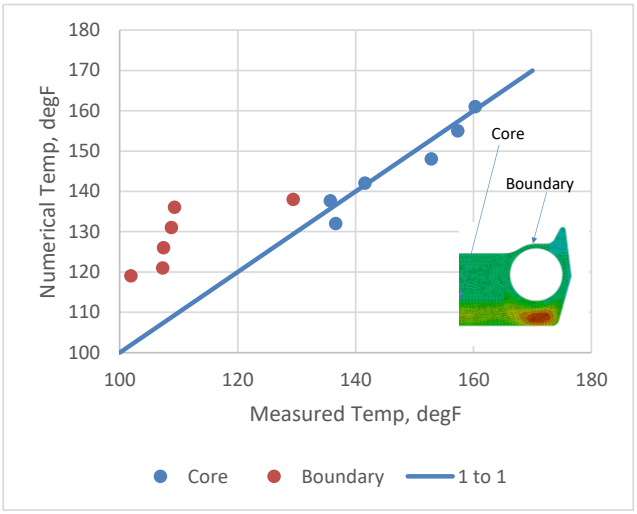

Figure 13. Computed steady-state temperature distribution for each operating case.

Fatigue Failure Modes

After fatigue testing, the track pads were sectioned and photographed to record failure modes. The typical failure mode for each operating condition is recorded in Figure 14.

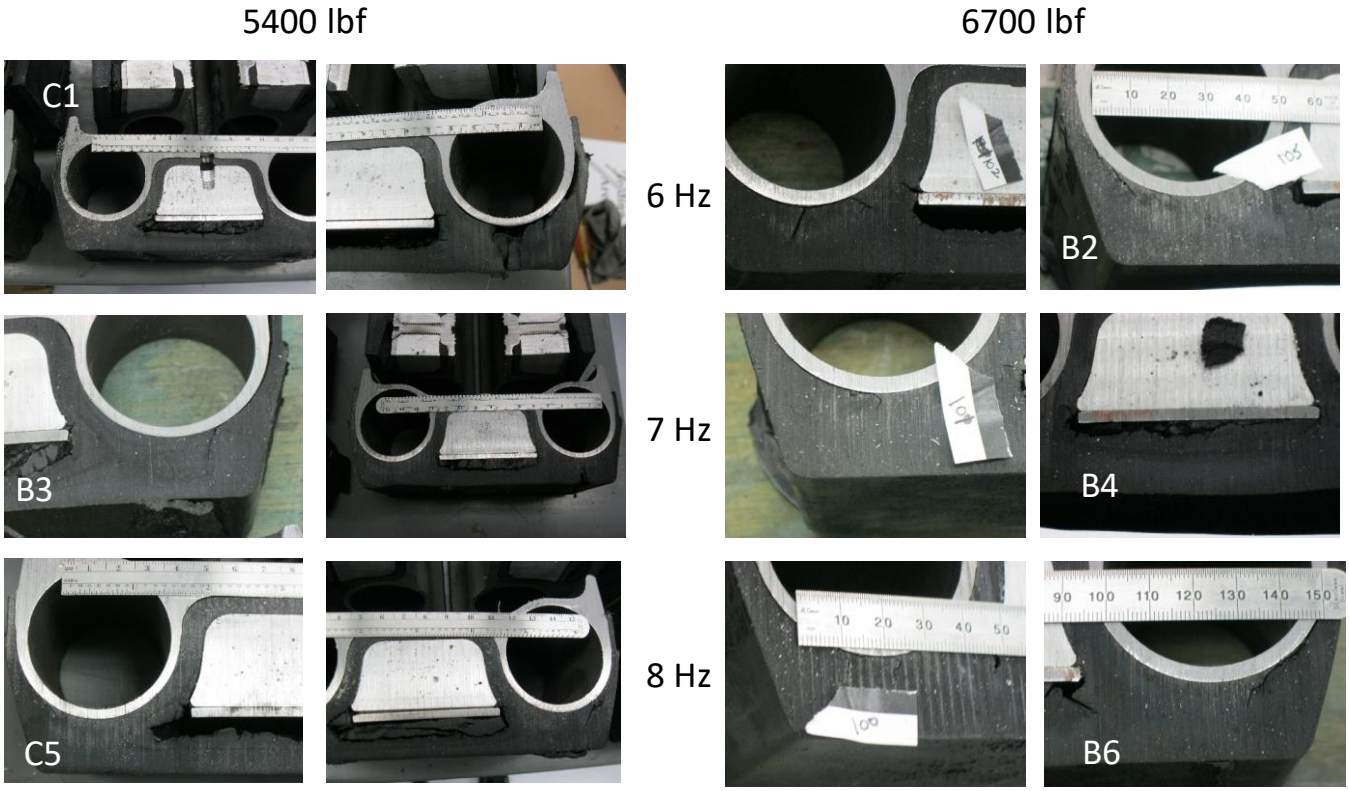

Figure 14. Track pad typical failure modes for each loading case.

Several distinct modes were observed. Cracking at locations predicted on the binocular tube and on the pad surface (at the point where the road wheel makes first contact with the pad) were observed. In addition, in some cases, a thermal runaway failure mode was also observed.

Thermal Runaway Failure Mode

In cases where thermal runaway occurred, core operating temperatures as high as 350 °F were recorded (the test was stopped whenever this failure mode occurred), and a thermal degradation mechanism was observed internally in the pad. The thermal runaway condition was found to be associated with a debond occurring between the elastomer and the steel insert covering the aluminum core. The debond resulted in very high heating rates arising due to friction between sliding crack faces. Figure 15 shows a thermal model that was run of the debonded condition. In this case, operating temperature continuously increases with no apparent upper bound until the elastomer completely degrades to a hard compacted powder with no load carrying capacity, as shown in Figure 16.

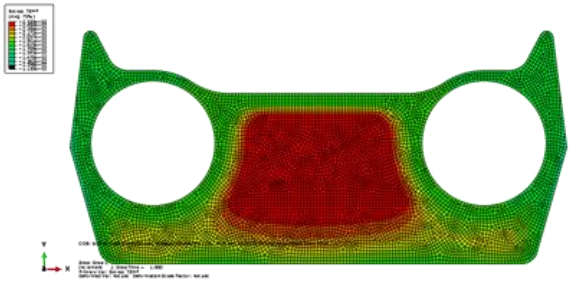

Figure 15. Computed temperature distribution for frictional heating due to debond between rubber and steel faceplate of the aluminum core. (blue = 113 °F, green = 183 °F, red= 252 °F).

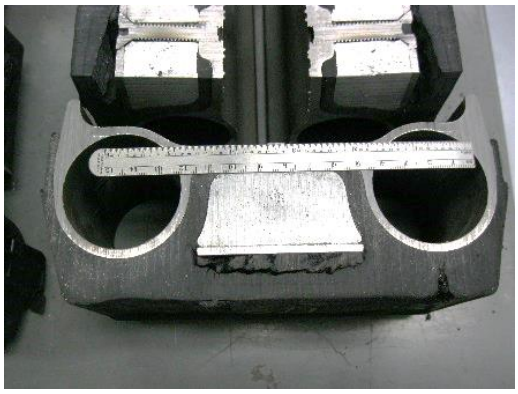

Figure 16. Track pad thermal runaway failure mode.

CONCLUSION

The digital twin of the backer pad component test yielded failure modes quite similar to those observed in experiments, and gave realistic estimates of operating temperature, failure mode and fatigue life.

The fatigue analysis methods developed under this project are now available commercially, and have proven effective in a wide range of elastomer applications beyond the backer pad application. Future applications of these tools will include durability improvement initiatives, light-weighting efforts, and remaining life tracking for reliability programs.

ABOUT ENDURICA

Endurica LLC provides solutions for managing durability of elastomers to automotive OEMs and rubber component developers. Our solutions include the Fatigue Property Mapping™ materials testing service, the fe-safe/Rubber™ and Endurica CL™ fatigue solver software packages, and Coesfeld fatigue testing instruments.

The Endurica CL fatigue solver is the only commercial fatigue code specialized for elastomers. It receives stress/strain/temperature history results obtained from a test or simulation, and accurately computes durability and remaining life. It takes into account the unique properties of rubber, and produces an accurate accounting of damage accrual under complex loading scenarios.

ACKNOWLEDGEMENT

The results in this report were generated under SBIR Phase II contract W56HZV-11-C-0202.

REFERENCES

[1]Mars, W. V., D. Ostberg. Fatigue Damage Analysis of an Elastomeric Tank Track Component. 2012 Simulia Community Conference, 2012.

[2]H.R. Brown, J.L. Bouvard, D. Oglesby, E. Marin, D. Francis, A. Antonyraj, H. Toghiani, P. Wang, M.F. Horstemeyer, M.P. Castanier, 2010 NDIA Ground Vehicle Systems Engineering and Technology Symposium, Modeling & Simulation, Testing, and Validation (MSTV) Mini-Symposium, August 17-19, Dearborn, Michigan.

[3]D. Ostberg and B. Bradford, “Impact of Loading Distribution of Abrams Suspension on Track Performance and Durability”, Proceedings of the 2009 Ground Vehicle Systems Engineering and Technology Symposium.

[4]Ogden, R. W. "Recent advances in the phenomenological theory of rubber elasticity." Rubber Chemistry and Technology 59, no. 3 (1986): 361-383.

[5]Yeoh, O. H. "On the Ogden strain-energy function." Rubber chemistry and technology 70, no. 2 (1997): 175-182.

[6]Li, X., Y. Wei. "Classic strain energy functions and constitutive tests of rubber-like materials", Rubber Chemistry and Technology 88, no. 4 (2015): 604-627.

[7]Ogden, R. W., and D. G. Roxburgh. "A pseudo–elastic model for the Mullins effect in filled rubber." In Proceedings of the Royal Society of London A: Mathematical, Physical and Engineering Sciences, vol. 455, no. 1988, pp. 2861-2877. The Royal Society, 1999.

[8]Mars, W. V. "Evaluation of a pseudo-elastic model for the Mullins effect." Tire Sci. Technol. 32, no. 3 (2004): 120-145.

[9]Gent, A. N., & Mars, W. (2013). Strength of elastomers. Science and technology of rubber, 419-454.

[10] Mars, W. V. 2007. "Fatigue life prediction for elastomeric structures." Rubber Chemistry and Technology 80, no. 3: 481-503.

[11] International Organization for Standardization, 2008. Rubber, Vulcanized — Measurement of Fatigue Crack Growth Rate. ISO 27727: Geneva, Switzerland.

[12] Rivlin, R. S., and A. G. Thomas. 1953. "Rupture of rubber. I. Characteristic energy for tearing." Journal of Polymer Science 10, no. 3: 291-318.

[13] Thomas, A. G. 1958. "Rupture of rubber. V. Cut growth in natural rubber vulcanizates." J. Polymer Sci 31, no. 123: 467-480.

[14] Mars, WV, Ellul MD, 2017. Fatigue Characterization of a Thermoplastic Elastomer, Rubber Chemistry and Technology, 90, no. 2.

[15] Aït-Bachir, M., Mars, W. V., Verron E, 2012. "Energy release rate of small cracks in hyperelastic materials." International Journal of Non-Linear Mechanics 47, no. 4: 22-29.

[16] Li, F, J. Liu, W. V. Mars, T.W. Chan, Y. Lu, H. Yang, L.Q. Zhang. "Crack precursor size for natural rubber inferred from relaxing and non-relaxing fatigue experiments." Int. J. Fatigue 80 (2015): 50-57.

[17] Luchini, J. R., Peters, J. M., Arthur, R. H., "Tire Rolling Computation with the Finite Element Method," Tire Sci. Technol., TSTCA, Vol. 22, 1994, pp. 206-222.

[18] Ebbott, T. G., Hohman, R. L., Jeusette, J-P., Kerchman, V., "Tire Temperature and Rolling Resistance Prediction with Finite Element Analysis," Tire Sci. Technol., TSTCA, Vol. 27, No. 1, January-March 1999, pp. 2-21.

[19] Terziyski, J. Kennedy, R., ‘‘Accuracy, Sensitivity, and Correlation of FEA-Computed Coastdown Rolling Resistance,’’ Tire Sci. Technol., TSTCA, Vol. 37, No. 1, January – March 2009, pp. 4-31.

[20] Meng-Jiao Wang, The Role of Filler Networking in Dynamic Properties of Filled Rubber, Rubber Chem. Technol. 72, 430, 1999

[21] Endurica CL v2.50 User Manual, 2017. Endurica LLC, Findlay, Ohio.

[22] Diani, J. "Directional constitutive laws for rubbers." Rubber Chemistry and Technology 89, no. 1 (2016): 22-31.

[23] Barbash, K. P., W. V. Mars. Critical Plane Analysis of Rubber Bushing Durability under Road Loads. No. 2016-01-0393. SAE Technical Paper, 2016.

[24] Goossens, J., Mars, W., Smith, G., Heil, P. et al., "Durability Analysis of 3-Axis Input to Elastomeric Front Lower Control Arm Vertical Ride Bushing," SAE Technical Paper 2017-01-1857, 2017.

[25] Mars, W. V. (2017). Computing Tire Component Durability via Critical Plane Analysis, Tire Science and Technology, 45 (in press).